

Fig. 3. Examples of images collected (A) on the ID30 beam line at ESRF with monochromatic 0.3738 Å radiation with the Fast Scan image plate, and (B) with in-house x-ray facilities at Uppsala Lab (Mo K α radiation, Smart CCD area detector) demonstrating the splitting of ferropericlasite reflections after long heating at temperatures above 950 K and pressures above 80 GPa. Inset shows backscattered electron image of the recovered sample (black, iron-rich parts; white, magnesium-rich parts).

width of the immiscibility gap in the MgO-FeO system at high pressure, nor can we determine whether ferropericlasite might dissociate completely into MgO and FeO after a sufficiently long time of heating. However, the ferropericlasites at least partially dissociate into a phase with lower density (Mg-rich, ~ 6.1 g/cm 3) and a phase with higher density (Fe-rich, ~ 7.8 g/cm 3) at 85 GPa, corresponding to a depth of 1900 to 2000 km (Preliminary Reference Earth Model). Such dissociation of ferropericlasite along with phase transitions in silica (23) and possible dissociation of (Mg,Fe)SiO $_3$ -perovskite (10, 17, 23) may lead to the heterogeneity of the lower mantle.

References and Notes

1. M. Rosenhauer, H. K. Mao, E. Woermann, *Yearb. Carnegie Inst. Washington* **75**, 513 (1976).
2. P. Richet, H. K. Mao, P. M. Bell, *J. Geophys. Res.* **94**, 3037 (1989).
3. D. G. Isaak, R. E. Cohen, M. J. Mehl, *J. Geophys. Res.* **95**, 7055 (1990).
4. Y. Fei, H. K. Mao, J. Shu, J. Hu, *Phys. Chem. Miner.* **18**, 416 (1992).
5. Y. Fei, *Am. Mineral.* **84**, 272 (1999).
6. ———, *Geochem. Soc. Spec. Pub.* **243** (1996).
7. ——— and H. K. Mao, *Science* **266**, 1678 (1994).
8. M. P. Pasternak et al., *Phys. Rev. Lett.* **79**, 5046 (1997).
9. R. E. Cohen, in *Review of High-Pressure Science and Technology*, M. Nakahara, Ed. (AIP Press, Kyoto, Japan, 1998), vol. 7, p. 160.
10. H. K. Mao, G. Shen, R. J. Hemley, *Science* **278**, 2098 (1997).
11. T. S. Duffy, R. J. Hemley, H. K. Mao, *Phys. Rev. Lett.* **74**, 1371 (1995).
12. Z. Fang, K. Terakura, H. Sawada, T. Miyazaki, I. Solovyev, *Phys. Rev. Lett.* **81**, 1027 (1998).
13. I. I. Mazin, Y. Fei, R. Downs, R. E. Cohen, *Mineralogy* **83**, 451 (1998).
14. R. E. Cohen, I. I. Mazin, D. G. Isaak, *Science* **275**, 654 (1997).
15. See *Science Online* (www.sciencemag.org/feature/data/1050995.shl).

16. J. Shu, H. K. Mao, J. Hu, Y. Fei, R. J. Hemley, *N. Jb. Mineral. Abh.* **172**, 309 (1998).
17. C. A. McCammon, A. E. Ringwood, I. Jackson, *Geophys. J. R. Astron. Soc.* **72**, 577 (1983).
18. At Uppsala Lab we have obtained powder x-ray diffraction data with a Siemens x-ray system consisting of a Smart charge-coupled device (CCD) area detector and a direct-drive rotating anode as x-ray generator (18 kW). The Mo K α radiation (tube voltage 50 kV, tube current 24 mA, cathode gun 0.1 \times 1 mm) is focused with a capillary x-ray optical system to 40 μ m full width at half-maximum. At ESRF we collected the powder diffraction data with a fine incident x-ray beam (approximately rectangular shape with dimensions 8 μ m by 9 μ m or less) of wavelength 0.3738 Å on the FastScan imaging plate. The collected images were integrated to obtain conventional diffraction spectra.

19. A. C. Larson and R. B. Von Dreele, *GSAS (General Structure Analysis System) LANSCE, MS-H805* (Los Alamos National Laboratory, Los Alamos, NM, 1994), p. 86.
20. S. Stolen, R. Glokner, F. Gronvold, T. Atake, S. Izumisa, *Am. Mineral.* **81**, 973 (1996).
21. E. Hälenius, H. Annersten, S. Jönsson, *Geochem. Soc. Spec. Pub.* **5** (1996), p. 255. Mössbauer experiments were performed using a conventional transmission geometry. Measurements were made on the quenched samples mounted on the diamond and leading the gamma rays through the gasket hole. A point source of ^{57}Co in Rh, nominal value 60 mCi, was used in the experiment and calibrated against α -Fe at room temperature.
22. Chemical analyses were obtained using the CAM-EBAX SX-50 electron microprobe with a phi-rho-Z correction procedure (operating conditions: accelerating potential, 20 kV; beam current, 50 nA; beam diameter, 1 to 2 μ m). Counting times were 10 s. The following analyzing crystals were used: TAP for Mg K α , Al K α , and Si K α ; LIF for Mn K α and Fe K α .
23. S. K. Saxena, P. Lazor, L. S. Dubrovinsky, *Mineral. Petrol.* **69**, 1 (2000).
24. Supported by the Swedish Natural Science Council and the Wallenberg and Crafoords Funds. The synchrotron x-ray studies were conducted at ESRF, Grenoble, on the ID30 beam line. The comments of two anonymous referees were useful.

6 March 2000; accepted 30 May 2000

Pattern of Marine Mass Extinction Near the Permian-Triassic Boundary in South China

Y. G. Jin,^{1*} Y. Wang,¹ W. Wang,¹ Q. H. Shang,¹ C. Q. Cao,¹ D. H. Erwin²

The Meishan section across the Permian-Triassic boundary in South China is the most thoroughly investigated in the world. A statistical analysis of the occurrences of 162 genera and 333 species confirms a sudden extinction event at 251.4 million years ago, coincident with a dramatic depletion of $\delta^{13}\text{C}_{\text{carbonate}}$ and an increase in microspherules.

The end-Permian mass extinction eliminated over 90% of all marine species and had a significant impact on land species as well (1, 2). However, geochronologic results from South China reveal that the main extinction occurred over a period of less than 500,000

years (3), coincident with the eruption of the Siberian flood basalts (4, 5) and with a sharp shift in $\delta^{13}\text{C}_{\text{carb}}$ (6). Although there are claims for multiple pulses of extinction, including at least three at the classic Meishan sections in South China (7, 8) [probably the most thoroughly studied Permian-Triassic (P-T) marine boundary section in the world], the cause of the extinction remains enigmatic. Here we examine sampling and preservation effects (9) using a statistical analysis of species' stratigraphic ranges (10, 11) to demonstrate the extreme rapidity of the extinction.

¹Nanjing Institute of Geology and Palaeontology, Academia Sinica, Nanjing 210008, China. ²Department of Paleobiology, MRC-121, National Museum of Natural History, Washington, DC 20560, USA.

*To whom correspondence should be addressed. E-mail: ygjin@public1.ptt.js.cn

REPORTS

We studied fossils systematically collected from five sections at the Meishan locality (12), at an average sample spacing of 30 to 50 cm. Smectite-rich clay beds occur frequently through the Changhsing and Yinkeng formations and can be traced across all outcrop areas. With the clay beds used as reference, a standard composite section was established for all fossil occurrences. We recorded a total of 333 species in 162 genera of 15 marine fossil groups, including foraminifera, fusulinids, radiolarians, rugosan corals, bryozoans, brachiopods, bivalves, cephalopods, gastropods, ostracods, trilobites, conodonts, fish, calcareous algae, and others from 64 horizons; the collection intensity was uniform, without any sampling gaps (Fig. 1).

About 161 species became extinct below the P-T boundary beds (beds 24 to 27). The extinction rate (extinct species divided by total species at the same level) does not exceed 33% in any bed of the Changhsing Formation below bed 24. The remaining species mostly disappeared within a short interval around the P-T boundary (beds 25 and 26), including the base of bed 25, where the extinction rate is 94%. We used confidence intervals on the end points of stratigraphic ranges (10, 14) and simulations for abrupt, gradual, and stepwise extinction scenarios (15) to evaluate the empirical pattern.

Confidence intervals were calculated for the stratigraphic ranges, measured in rock thickness, of the 93 genera (265 species; 80%

of the total species) with multiple occurrences. The range end points of 95% confidence intervals for more than 95% of the genera extend into bed 34 of the Yinkeng Formation. Calculated depositional rates between the radiometrically dated ash beds (3) are 0.03 cm per 1000 years for the transitional beds versus 0.4 cm per 1000 years for the upper part of the Changhsing Formation and 1.3 cm per 1000 years for the basal part of the Yinkeng Formation. The idea that deposition occurred by a slow sedimentation process is supported by extensively burrowed hardgrounds within bed 27 (16). Thus the forward smearing of the confidence intervals was likely produced by the condensed transitional sequence from beds 24e to 27.

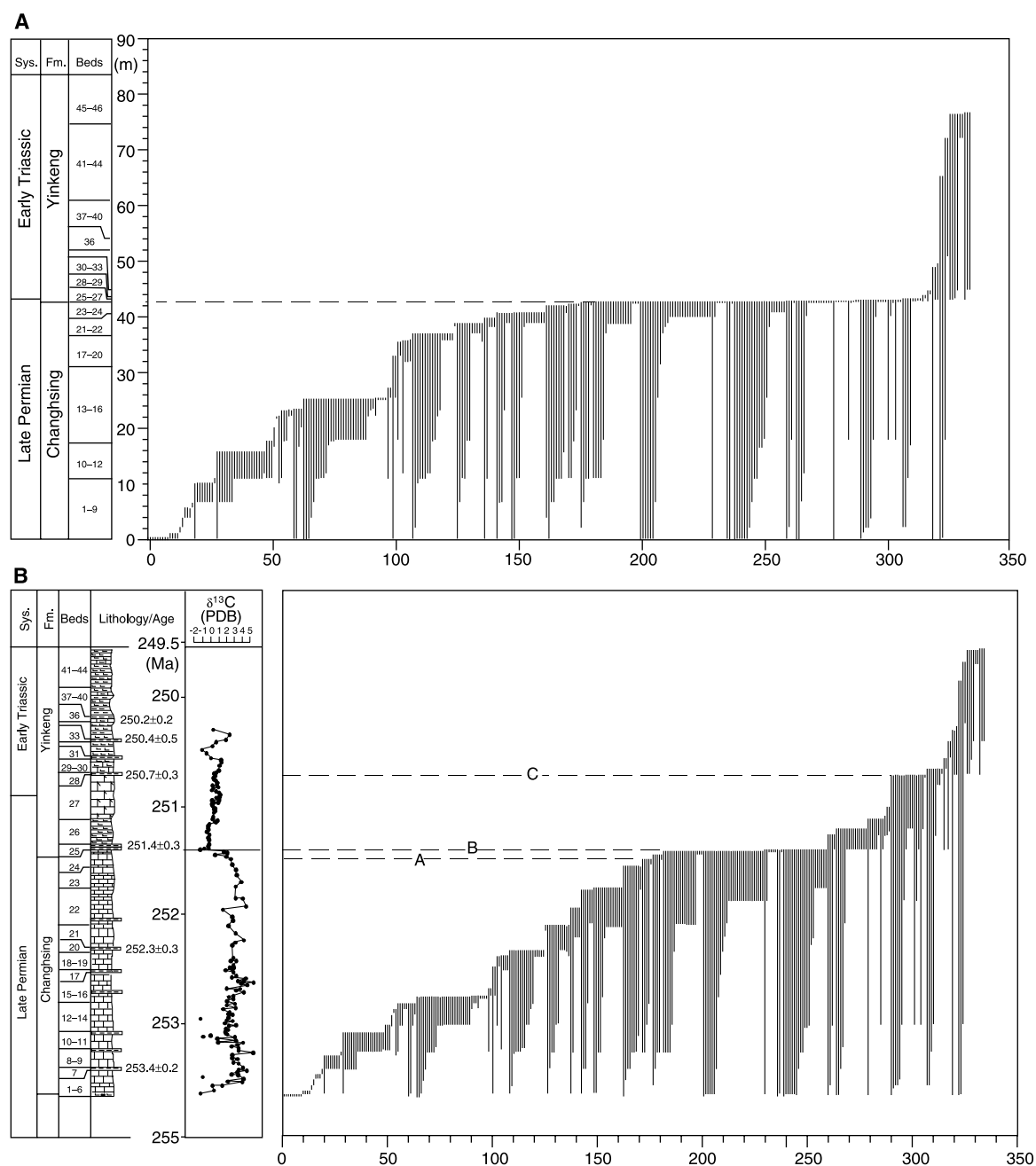


Fig. 1. Stratigraphic ranges of fossil species (indicated by vertical gray lines) from the latest Permian to the Early Triassic in the Meishan sections projected onto the composite section. Species numbers are shown on the x axes. **(A)** Fossil range scaled to rock thickness, with an abrupt faunal change near the base of bed 25. **(B)** Fossil range scaled to time. Faunal change appears gradual except around 251.4 Ma. The positions of volcanic ash beds and isotopic ages are from (3). The $\delta^{13}\text{C}_{\text{carb}}$ profiles integrate all available data from the Meishan sections (8, 20, 21). Three previously proposed extinction levels are shown (indicated by A, B, and C) (24).

To assess the true timing of the events, we assumed a linear deposition rate in the intervals bracketed by the dated ash beds, which accounts for these variations in sedimentation rates. We calculated the ages of each fossil occurrence, the number of fossil horizons, the time interval from the last observed occurrence to the postulated extinction horizon (α), and confidence levels (ρ) associated with each α value for all genera (10, 14). A Kolmogorov-Smirnov test does not reject the null hypothesis: The confidence levels are independently uniformly distributed between $\rho = 0$ and $\rho = 1$. The distribution of last occurrences suggests an extinction peak between 251.2 and 251.4 million years ago (Ma). The 50% confidence intervals on the stratigraphic ranges of all 93 genera are consistent with a sudden extinction around 251.4 Ma (13) (Fig. 2A), with a predicted true extinction level near 251.3 Ma [94% of genera are included in a 0.1-million-year (My) interval spacing]. A more reasonable conclusion, equally consistent with the statistical analysis, is a sudden extinction at 251.4 Ma, followed by the gradual disappearance of a small number of surviving genera over the next 1 million years.

We repeated the analysis for the 38 genera that cross the P-T boundary to test for a second extinction peak. The predicted extinction is at 250.6 Ma, with a confidence of 95.1% for a 0.5-My interval spacing, declining to 55% for a 0.1-My spacing; the broad spacing of final occurrences does not support a sudden extinction after the P-T boundary. A similar analysis for genera that disappeared before 251.4 Ma provides no support for an earlier extinction step at bed 24e (17).

Several groups were analyzed individually. Fifty percent confidence intervals for 15 of 22 foraminifer genera and 13 of 21 ostracod genera indicate a sudden extinction near 251.4 Ma. Fifty percent confidence intervals for conodont genera (platform elements) and bivalves show a gradual change. The predicted position of the true extinction horizons for the foraminifera, ostracods, and cephalopods is around 251.4 Ma (Fig. 2, B through D). In contrast, 50% confidence intervals for 6 of 13 brachiopod genera display a sudden extinction at 250.6 Ma (Fig. 2E). Despite this apparent latter extinction of brachiopods, they are not well preserved in this slope facies. A P-T boundary section 27 km east of Meishan in a shallow shelf facies contains 18 brachiopod genera between the sequence boundary and the boundary clay. As with the foraminifera, ostracods, and cephalopods at Meishan, the brachiopods suffer dramatic decline at the boundary clay and a secondary extinction at the level corresponding to 250.6 Ma.

Simulations of sudden extinctions produce an accelerating decline in the number of taxa, whereas gradual extinctions display a constant decline, and stepwise extinctions display a

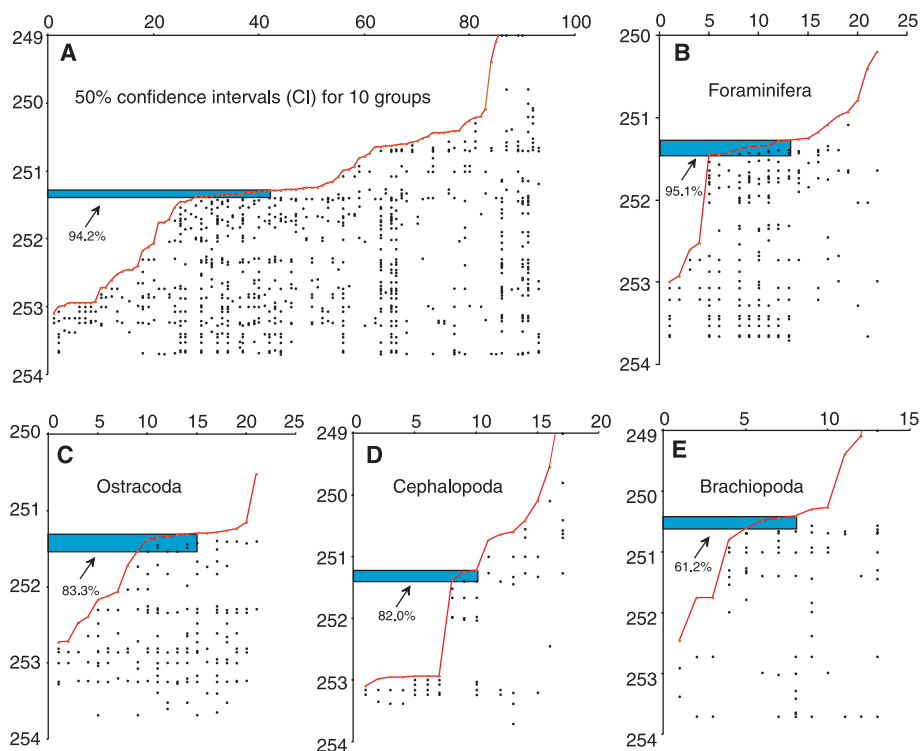


Fig. 2. (A) Fifty percent confidence intervals [the interval between red dots (confidence end points) and last occurrences (upper black dots)] for 93 genera of 10 different groups (foraminifera, fusulinids, bryozoans, brachiopods, rugosan coral, bivalves, cephalopods, ostracods, conodonts, and calcareous algae) with multiple occurrences at the composite P-T section at Meishan. Fifty percent confidence intervals for the foraminifera (B), ostracod (C), cephalopod (D), and brachiopod (E) genera are shown separately. Time (in Ma) is shown on the y axes; numbers on the x axes indicate species number. Contours indicating the predicted extinction level are shown for each group (blue bars); the probability that the extinction lies within each interval is given below the intervals. The probability was defined by iteratively eliminating genera that fall beyond the extinction level at the 99.99% level. The apparent brachiopod extinction at 250.6 Ma may reflect the scarcity of fossils below the boundary beds; the occurrences of ammonoids, conodonts, bivalves, and other groups are also spotty. Ammonoids exhibit stepped declines at 253.0 and 251.4 Ma.

stepped decline (15). We plotted the age of last occurrences versus stratigraphic abundance (percentage of the time intervals during which a genus occurs divided by the total number of occurrences) for all 162 genera as well as for each group. The results for all 162 genera show a sudden extinction near 251.4 Ma, followed by a gradual decline from 251.4 to 250.6 Ma. The results for foraminifera and ostracods display the hollow shape typical of a sudden extinction (Fig. 3A). Individual exceptions include the ostracod genera *Acratia* (30% abundance) and the foraminifer *Pseudonodosaria* (20%), which extend beyond the P-T boundary elsewhere in South China (18). The number of last occurrences by time has a single mode (Fig. 3B). The fossil occurrences at Meishan are best explained by a major extinction around 251.4 Ma. No support is found for previously proposed extinction steps related to the end of the Paleozoic reef system correlative with bed 24e or the extinction of relic Paleozoic brachiopods at bed 28. However, an increase in fungal spores, a possible indicator of massive disturbance in the terrestrial ecosystem, begins below bed 24 (19).

Significant negative $\delta^{13}\text{C}$ anomalies have

been reported from the extinction interval at Meishan (6, 20). These include a drop in $\delta^{13}\text{C}$ value from +2 to -4 per mil (‰) within bed 26, and to -6‰ at the basal levels of bed 27 (20). New $\delta^{13}\text{C}_{\text{carb}}$ data from section B (21) confirm a depletion of $\delta^{13}\text{C}$ in beds 25 and 26 but not the reported depletion in bed 27 (Fig. 4). The accompanying $\delta^{18}\text{O}$ values, ranging from -8 to -11‰ (21), indicate that the previously reported unusually low $\delta^{13}\text{C}$ values in basal bed 27 might reflect strong weathering. The carbon isotope shift from the top of bed 24e to the lower part of bed 26 is consistent with a major extinction event around 251.4 Ma and the addition of light carbon.

Unlike the illite ash clay beds above and below the P-T boundary, the boundary clay beds are dominated by interstratified montmorillonite-illite clay (22). P-T boundary levels in South China are accompanied by concentrations of microspherules that are 10^2 to 10^3 times those of other horizons (8, 23); many of these appear to be volcanic, although the mechanism remains uncertain (7). The peak microspherule abundance is not neces-

REPORTS

Fig. 3. Results for simulations of 162 genera from the Meishan sections. (A) Frequency distribution of last occurrences for 162 genera and for foraminifer, ostracod, cephalopod, and brachiopod genera, respectively. (B) Histograms plotted by the total number of time intervals at which a genus occurs versus the age of last occurrence. Only genera of less than 15% stratigraphic abundance tend to have last occurrences well below the major extinction time of 251.4 Ma; genera of exception are indicated by names in (A). The genera that extend upward beyond 250 Ma are not plotted in the figure. Each dot may represent more than one genus with the same coordinate position.

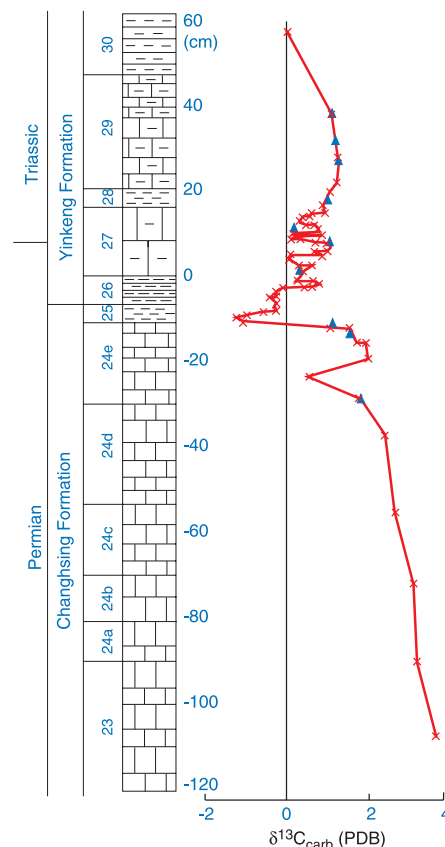
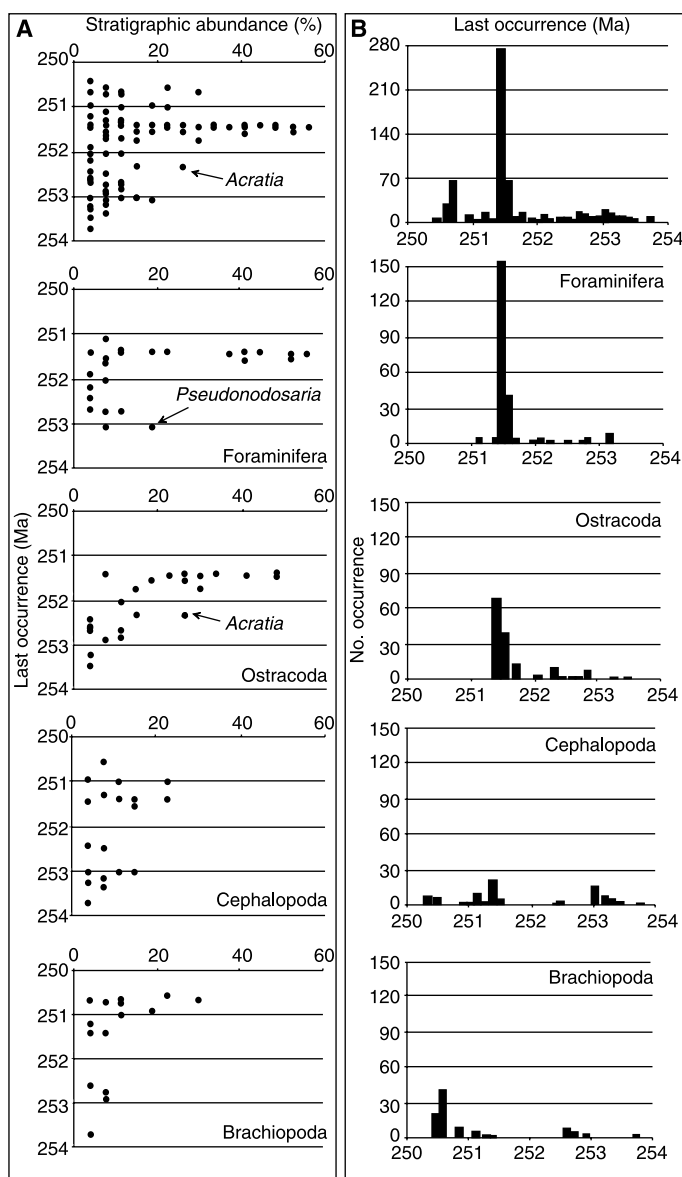


Fig. 4. Carbon isotope profile of P-T boundary interval at section B of Meishan. Blue triangles represent replicate results of the same samples, provided by S. D'Hondt (28).

sarily associated with an ash-clay layer. In the Shangsi section in Sichuan Province, the microspherule concentration increases rapidly from the white ash-clay layer coincident with the mass extinction (bed 27b) to a peak in the black shale of bed 27c (23).

In the Meishan sections, three successive transgression surfaces are closely associated with hypothesized biotic downturns (24). Evidence for anoxia at Meishan includes pyritic laminae beneath bed 25 and a reduction in trace fossils in P-T boundary beds (13). Other, more reliable evidence of bottom oxygenation does not indicate drastic anoxia in association with the severe extinction in bed 25. Framboidal pyrites are rare, and total organic carbon (TOC) is relatively low in beds 26 and 27 (25), although well-developed framboidal pyrites and high percentages of TOC appear in organic-rich levels of beds 24 and 29. Bed 26 contains the trace fossil *Planolites*

and bed 27 was thoroughly burrowed by *Thalassinoides* (16). The scenario of transgression with anoxia appears unable to explain the severe extinction in bed 25.

Both pyroclastic and flood basalt volcanism have been invoked as causes for the extinction (4, 7). The temporal overlap between the Siberian Trap volcanism (251.2 ± 0.3 Ma) and the P-T boundary (<251.5 and >250.5 Ma) suggests a causal relation (3, 5, 26). The Siberian flood basalt may have released large amounts of CO_2 , and possibly sulfates, triggering a brief volcanic winter, followed by a period of global warming (5, 27). The frequent acidic volcanism from the latest Permian to the earliest Triassic in South China has been invoked as a causal factor (7, 26), but the lack of extinction at most ash beds augurs against any simple relation (1). The rapid marine extinction in bed 25 is consis-

tent with the dramatic shift of carbon isotopic data and coincides with the microspherule anomaly. Despite the lack of compelling evidence for extraterrestrial impact, the rapidity of the extinction and the associated environmental changes are also consistent with the involvement of a bolide impact in this most severe biotic crisis in the history of life.

References and Notes

1. D. H. Erwin, *The Great Paleozoic Crisis: Life and Death in the Permian* (Columbia Univ. Press, New York, 1993).
2. G. J. Retallack, *Science* **267**, 77 (1995).
3. S. A. Bowring et al., *Science* **280**, 1039 (1998).
4. I. H. Campbell, G. K. Czamanske, V. A. Fedorenko, R. L. Hill, V. Stepanov, *Science* **258**, 1760 (1992).
5. P. R. Renne, Z. Zhang, M. A. Richardson, M. T. Black, A. R. Basu, *Science* **269**, 1413 (1995).
6. A. Baud, M. Magaritz, W. T. Holser, *Geol. Rundsch.* **78**, 649 (1989).
7. H. F. Yin, in *Permo-Triassic Events in the Eastern Tethys*, W. C. Sweet, Z. Y. Yang, J. M. Dickens, H. F. Yin, Eds. (Cambridge Univ. Press, Cambridge, 1992).
8. Z. Y. Yang et al., *Permo-Triassic Events of South China* (Geological Publishing House, Beijing, 1993).
9. P. W. Signor III and J. H. Lipps, *Geol. Soc. Am. Spec. Pap.* **190**, 291 (1982).
10. C. R. Marshall, *Paleobiology* **20**, 459 (1994).
11. ——— and P. D. Ward, *Science* **274**, 1360 (1996).
12. J. K. Zhao et al., *Bull. Nanjing Inst. Geol. Palaeontol. Acad. Sin.* **1**, 95 (1981); Sheng et al., *J. Fac. Sci. Hokkaido Univ.* **21**, 133 (1984). The P-T boundary

interval at Meishan occurs during the transition from the latest Permian Changhsing Formation to the Earliest Triassic Yinkeng Formation. The Changhsing Formation is composed of graded beds of organic-rich calcarenite, marly micrite, and radiolarian chert, representing slope-to-basinal facies (73). A third-order sequence boundary surface occurs 20 cm below the top of the Changhsing Formation, with the topmost 20 cm of lime mudstone (bed 24e) representing a shelf margin system tract. Bed 24e is overlain by a transitional sequence of about 28 cm with a sharp contact. It consists of a pale-colored, alternated ash clay bed (bed 25) below, a laminated organic-rich calcareous claystone (bed 26) in the middle, and a 16-cm lime mud bed above (bed 27). Bed 26 contains rare but highly diverse skeletal fossils, including the earliest Triassic ammonoid *Otoceras*. Bed 27 includes an extensively burrowed hardground 5 cm above its base and discontinuous hardgrounds in its upper part (16). The first occurrence of the conodont *Hindeodus parvus* between bed 27c and bed 27b at section D of Meishan has been proposed as the biostratigraphic P-T boundary. Overlying the transitional sequence are graded beds ranging from gray organic-rich shale to pale marls or muddy limestone. The earliest postulated extinction event (7, 8) is referred to the elimination of latest Permian reefs in South China, which corresponds to the base of bed 24e at Meishan. The second event is the disappearance of most benthos at beds 25 and 26, and the final event is the disappearance of the final few Permian brachiopods at bed 28.

13. P. B. Wignall and A. Hallam, *Palaeogeogr. Palaeoclimatol. Palaeoecol.* **102**, 215 (1993).
 14. M. S. Springer, *Paleobiology* **16**, 512 (1990). Confidence intervals on the apparent stratigraphic range of selected taxa were calculated from $C_1 = 1 - (1 + r/R)^{-(H-1)}$, where C_1 is the confidence level, r is the size of the confidence interval, R is the observed stratigraphic range, and H is the number of known fossil horizons (12). Because confidence intervals with $H < 2$ would be of little value, 59 genera with single occurrences were excluded, as were four foraminiferal and six conodont genera ranging throughout the section. The predicted positions of the true extinction horizons for 93 genera and for foraminifer, ostracod, and brachiopod genera, assuming there is one for each case, were computed separately. All genera with confidence values higher than 95% for disappearance well below the bottom of bed 24 (the boundary level) were eliminated. Using the binomial distribution, we calculated the 99% confidence envelope and eliminated genera with confidence intervals beyond the envelope. This process was repeated for the remaining genera, with the predicted true extinction horizon lying between the intervals.
 15. K. H. Meldahl, *Geology* **18**, 890 (1990).
 16. C. Q. Cao and Q. H. Shang, *Palaeoworld* **9**, 147 (1998).
 17. The predicted true extinction level before 251.4 Ma is at 252.6 Ma with 96% confidence for a 0.6-My spacing but only 46.8% for a 0.1-My spacing.
 18. W. C. Hao, *J. Geosci. Osaka City Univ.* **39**, 19 (1994).
 19. S. Ouyang and J. Utting, *Rev. Palaeobot. Palynol.* **66**, 65 (1990).
 20. Z. Yan, D. Xu, L. F. Ye, R. M. Lu, *Palaeoworld* **1**, 113 (1989).
 21. Twenty-milligram samples were recovered with a microdriller for each point and were reacted with 100% H_3PO_4 at 25°C for 8 hours. Samples were analyzed in a Finnegan MAT 251 mass spectrometer for $\delta^{13}C$ and $\delta^{18}O$, using the Chinese national standard, an Ordovician carbonate from a site near Beijing [reference number GBW 04405: $\delta^{13}C = 0.57 \pm 0.03$ Pee Dee belemnite (PDB); $\delta^{18}O = -8.49 \pm 0.13$ PDB]. Analysis of a weathered specimen from bed 27 produced $\delta^{13}C$ values ranging from -3.6 to -4.2% and $\delta^{18}O$ values ranging from -8.2 to 12.6% .
 22. F. Asaro, L. W. Alvarez, W. Alvarez, H. V. Michel, *Geol. Soc. Am. Spec. Pap.* **190**, 517 (1982).
 23. Z. G. Gao, D. Y. Xu, Q. W. Zhang, Y. Y. Sun, *Geol. Rev.* **33**, 203 (1987). Microspherules from boundary clay beds range from 50 to 300 μm , and most average 100 μm in diameter. Ninety-five percent are spherical; a few are oval, teardrop-shaped, or consist of two fused spheres. Ninety percent are ferruginous,

black, metallic, and strongly magnetic, with delicate surface projections. X-ray analysis suggests that they are possibly composed of magnesioferrite and hematite, but one spherule is chromespinel (7). Ten percent are glassy and range from colorless to yellowish, brownish, or semitransparent. These spherules are isotropic in polarized light, with smooth, individually reticulate, or pitted surfaces. No phenocrysts or microoliths of high-temperature minerals have been found in the glassy spherules. Both kinds of spherules may bear vesicles. Microprobe analysis indicates less than 0.1% Cr_2O_3 , SO_3 , and NiO in both kinds of spherules. Glassy spherules contain SiO_2 , 34.6 to 54.9%; Al_2O_3 , 4.9 to 17.8%; FeO, 4.8 to 11.0%; CaO, 11.5 to 36.1%; and MgO, 0.5 to 3.0%. Ferruginous spherules contain SiO_2 , 48.0 to 29.5%; Al_2O_3 , 15.8 to 22.7%; FeO, 40.9 to 80.3%; CaO, 0.7 to 2.7%; and MgO, 1.2 to 3.1%. In ferruginous spherules, amounts of SiO_2 and CaO are lower than in glassy spherules, and K_2O is entirely absent.

24. K. X. Zhang *et al.*, in *The Palaeozoic-Mesozoic Boundary*, H. F. Yin, Ed. (China Univ. of Geology Press, Wuhan, 1996).
 25. C. Q. Cao, thesis, Nanjing Institute of Geology and Palaeontology, Nanjing, China (1999).
 26. J. W. He, L. Rui, C. F. Chai, S. L. Ma, *J. Stratigr.* **11**, 194 (1987).
 27. H. Visscher *et al.*, *Proc. Natl. Acad. Sci. U.S.A.* **93**, 2155 (1996).
 28. S. D'Hondt, personal communication.
 29. We appreciate discussions and comments from S. D'Hondt and C. Marshall and comparative $\delta^{13}C$ data from S. D'Hondt. Supported by the NSF China Grant 49672092, the Ministry of Science and Technology China Basic Research Projects G99-A-05b and G2000077705, Academia Sinica grant K2951-B1-409, and the NASA Exobiology Program and National Astrobiology Institute (to D.H.E.).

21 March 2000; accepted 30 May 2000

Negative Regulation of the SHATTERPROOF Genes by FRUITFULL During Arabidopsis Fruit Development

Cristina Ferrándiz,* Sarah J. Liljegren,* Martin F. Yanofsky†

The terminal step of fruit development in *Arabidopsis* involves valve separation from the replum, allowing seed dispersal. This process requires the activities of the SHATTERPROOF MADS-box genes, which promote dehiscence zone differentiation at the valve/replum boundary. Here we show that the FRUITFULL MADS-box gene, which is necessary for fruit valve differentiation, is a negative regulator of SHATTERPROOF expression and that constitutive expression of FRUITFULL is sufficient to prevent formation of the dehiscence zone. Our studies suggest that ectopic expression of FRUITFULL may directly allow the control of pod shatter in oilseed crops such as canola.

The fruit mediates the maturation and dispersal of seeds and is derived from the female reproductive structure, the gynoecium. The *Arabidopsis* fruit, which is typical of more than 3000 species of *Brassicaceae*, consists of an apical stigma, a short style, and a basal ovary that contains the developing seeds (Fig. 1A). The peripheral walls of the fruit are referred to as valves and are connected on both sides by a thin structure known as the replum. At the valve/replum boundary, a narrow band of cells differentiates into the dehiscence zone (1), where the separation of cells late in fruit development allows valve detachment from the replum and seed dispersal.

Because FRUITFULL (*FUL*) is required for the expansion and differentiation of fruit valves after fertilization (2), we generated transgenic plants in which *FUL* is constitu-

tively expressed from the cauliflower mosaic virus 35S promoter (3–5) to determine if *FUL* is sufficient to specify valve cell fate in ectopic positions. The most striking phenotype caused by the 35S::*FUL* transgene is the conversion of cells within the valve margin and outer replum to valve cells (Fig. 1). Consequently, the dehiscence zone, which normally forms at the valve margin (Fig. 1, A and C), fails to differentiate in 35S::*FUL* fruit (Fig. 1, B and D). Thus, like *shatterproof* (*shp1 shp2*) loss-of-function mutants (6), 35S::*FUL* gain-of-function plants produce indehiscent fruit and fail to disperse their seeds normally.

Because lignification is thought to play an important role in the dehiscence process (1), and because the *SHP* genes promote lignification of cells adjacent to the dehiscence zone (6), we examined the lignification patterns of 35S::*FUL* and *ful* fruit compared with that seen in the wild type (7). Whereas only a single valve cell layer is lignified in wild-type fruit (Fig. 1E), all of the internal valve mesophyll layers also become lignified in *ful* fruit (Fig. 1G). Correspondingly, in 35S::*FUL* fruit (Fig. 1F), we found a consis-

Section of Cell and Developmental Biology, University of California at San Diego, La Jolla, CA 92093-0116, USA.

*These authors contributed equally to this work.

†To whom correspondence should be addressed. E-mail: marty@ucsd.edu